AIAA JOURNAL
Vol. 35, No. 7, July 1997

Natural Coherent Structure Dynamics in Near Field of Fully Turbulent Axisymmetric Jet

S. Aydore*
Istanbul Technical University, Istanbul 80626, Turkey
and
P. J. Disimile†
University of Cincinnati, Cincinnati, Ohio 45221-0070

Natural coherent structures in the near field of an axisymmetric jet have been educed, and their dynamics studied experimentally using hot-wire anemometry. The jet, originating from a fully developed turbulent pipe flow, was positioned four jet diameters upstream from an impingement plate. Based on the pipe diameter, a jet Reynolds number of 1.3×10^4 was maintained. Using the life cycle method for coherent structure eduction, phased-averaged vorticity contours were obtained in the jet near field, within 2.3 diameters of the pipe exit. Vorticity contours suggest that large coherent structures exist in the middle of the shear layer at approximately one jet diameter downstream from the pipe exit. Their size, 40% of the initial jet diameter, is maximum at this location. A decay region was also observed 1.6 diameters downstream from the pipe exit. Individual terms in the coherent vorticity equation were evaluated and significant terms examined.

Nomenclature

D	= jet (or delivery tube) diameter
f_m	= dominant passage frequency, Hz
i	= phase point, e.g., i is equal to 1 the first time interval in the cycle
L	= pipe exit to plate spacing
P	= time-averaged shear production
$\langle P \rangle_i$	= phase-averaged shear production at the ith phase point
R	= radial direction
R/D	= normalized radial distance
S	= time-averaged strain rate
$\langle S \rangle_i$	= phase-averaged strain rate at the ith phase point
t	= time
U	= time-averaged longitudinal velocity
U_{cl}	= time-averaged centerline pipe exit velocity
$\langle U_C \rangle$	= phase-averaged convection velocity
$\langle U \rangle_i$	= phase-averaged longitudinal velocity at the ith phase point
u'	= longitudinal turbulent velocity component
$\langle u' \rangle_i$	= phase-averaged longitudinal turbulent velocity component at the ith phase point
$u'v'$	= Reynolds stress
$\langle u'v' \rangle_i$	= phase-averaged Reynolds stress at the ith phase point
$\langle V \rangle_i$	= phase-averaged transverse velocity at the ith phase point
v'	= transverse turbulent velocity component
$\langle v' \rangle_i$	= phase-averaged transverse turbulent velocity component at the ith phase point
X	= streamwise direction
X/D	= normalized streamwise distance
Θ	= circumferential direction
ω	= time-averaged transverse vorticity, in z direction
$\langle \omega \rangle_i$	= phase-averaged transverse vorticity at the ith phase point
$'$	= random fluctuating part
$\langle\rangle$	= phase averaged

Received Aug. 21, 1995; revision received March 3, 1997; accepted for publication March 26, 1997.

*Assistant Professor, Aeronautical Engineering Department.
†Bradley Jones Associate Professor, Department of Aerospace Engineering and Engineering Mechanics, ML#70. Member AIAA.

Introduction

LARGE-SCALE coherent structures are known to exist and be responsible for most of the momentum, heat, and mass transfer in turbulent flows. With an increased knowledge of the coherent structures present in jet flows undergoing impingement, optimum heat transfer systems can be built for industrial applications, such as cooling of electronic components and aircraft turbine blades.

Coherent structures have been identified in several flow visualization studies performed in free shear flows.[1] Usually, laminar flow conditions and low Reynolds numbers provide sufficient flow stability to ensure good visual resolution, and with that the evidence of coherent structure existence is supplied. However, when the Reynolds number is high, most flow visualization techniques fail to identify the coherent structures, although they are readily present in the flowfield. This difficulty in flow visualization at high Reynolds numbers is inevitable because of the smearing that takes place within the large-scale structures due to the increased presence of fine grained turbulence.[2] Coherent structure visualization is particularly difficult in fully turbulent jet flows due to the three dimensionality of the structures and the rapid diffusion of fluid markers caused by small-scale turbulence.[3]

Hussain[4] states that the instability of the instantaneous profile (not the mean profile) should be able to explain the coherent structure formation. Therefore, the current phase-averaged (time-dependent) measurements are also appropriate for the study of vortex formation. Tso and Hussain[5] suggest that coherent structure formation and growth should occur in the valleys of shear production. Many studies have also noted that the jet near field is dominated by the jet tone instabilities and these local instabilities are known to initiate the evolution of the coherent structures.[4,6–8]

Eduction of large-scale coherent structures requires the acquisition of detailed quantitative data on such structure characteristics as size, strength, convection velocity, etc. The eduction of the coherent structures is rather difficult, time consuming, and paradoxical.[4] The difficulty arises due to the use of point measurements instead of simultaneous full field measurements. Although particle image velocimetry is making progress, this technique has only had limited success in low Reynolds number flows, i.e., less than 1.5×10^4. Inasmuch as it is impossible (at least for now) to acquire data at each of the measurement points simultaneously, without physically disturbing the flowfield, coherent structures must be educed using separate point measurements. Applying a predetermined selection criterion, these individually acquired signals can be event or phase aligned with one another. Such a strategy allows ensemble averaging of the

signals and a determination of desired phase-averaged flow quantities. In the present study, the acquisition of conditionally sampled time series at many spatial locations has enabled the determination of phase-averaged flow quantities and allowed the reconstruction of the coherent flowfield. This has enabled the time evolution of vortex formation, growth, and downstream convection of the natural large-scale structures within the shear layer to be investigated.

Experimental Apparatus and Measurement Strategy

Air for the jet was supplied by a compressed air storage system. The air initially stored at high pressure was reduced in pressure and directed to an obstruction type flowmeter. After exiting the flowmeter, the air was introduced into a 45-diam-long, vertically oriented circular delivery tube (or pipe) of inner diameter 5.08 cm, via a flexible hose. The flow rate was set and maintained at a constant level to within $\pm 2\%$, ensuring that the jet velocity (U_{cl}) at the delivery tube exit remains fixed at 4 m/s during the experiment. Because neither a settling chamber nor a nozzle was utilized and the tube was of sufficient length, a fully turbulent pipe flow was obtained at the jet origin. Figures 1a and 1b represent the normalized velocity and streamwise component of turbulence intensity $1D$ downstream from the delivery tube exit. Upon exiting the delivery tube, the jet was able to spread and impinge on a flat plate. The impingement length characterized by the jet to plate spacing, L/D, was set to 4.

Using constant temperature anemometry and an X-wire probe, velocity measurements throughout the flowfield were acquired. The active region of the probe was formed with two 4-μm tungsten wires 3 mm in length and separated by a 1-mm spacing. Each wire was oriented at an angle of 55 deg with respect to the probe axis.

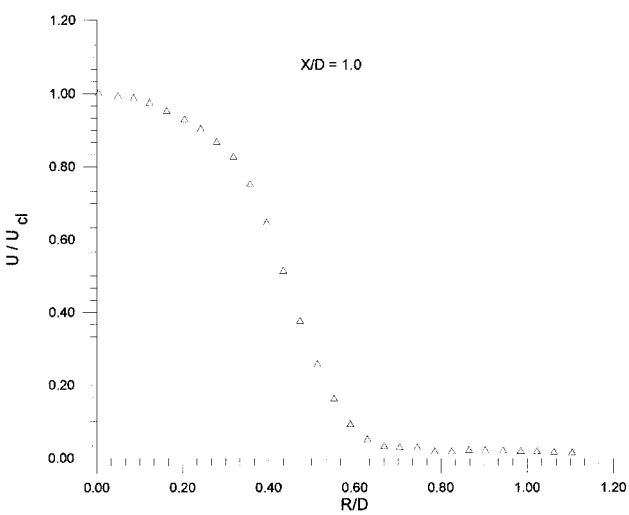

Fig. 1a Time-averaged normalized streamwise velocity profile.

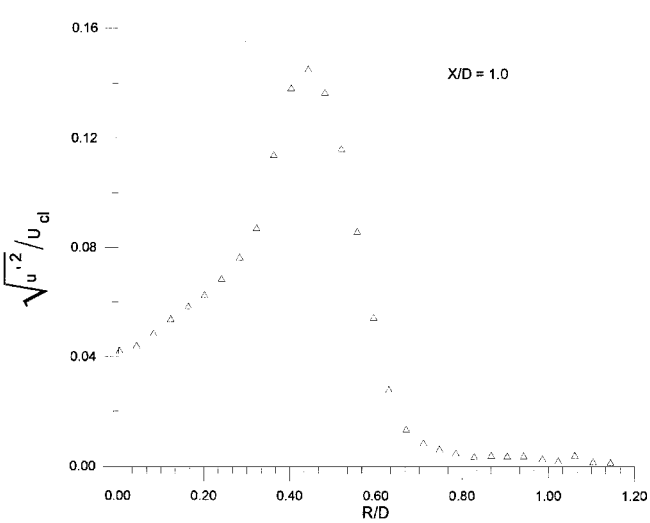

Fig. 1b Normalized streamwise turbulence intensity profile.

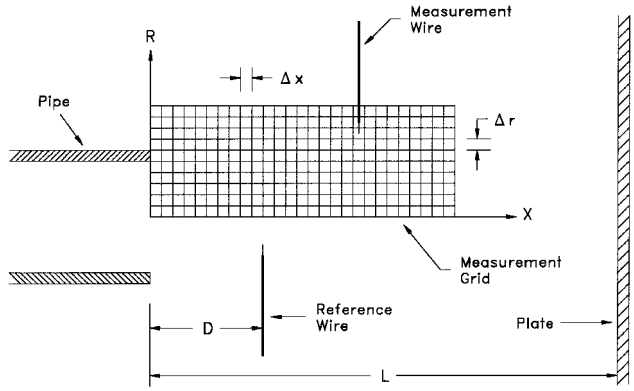

Fig. 2 Experimental configuration and measurement grid.

The calibration of the X-wires was performed using the calibration procedure of Foss et al.[9] This strategy calibrates the wires at 15 angles with respect to the incoming flow and seven speeds from 0.1 to 5.0 m/s for each angle.

A reference probe, used to detect the passing of vortical motions, consisted of a single straight 4-μm tungsten wire. After extensive fast Fourier transform (FFT) surveys, the reference probe was positioned in the flowfield at $X/D = 1.0$ and $R/D = 0.25$. To minimize reference probe interference, the X-wire probe was positioned on the opposite side of the jet (see Fig. 2). Analog signals provided by the three anemometers were sampled simultaneously in 0.5-ms intervals using a 12-bit multichannel A/D converter. A measurement plane formed by the jet centerline and delivery tube exit plane extended $2.3D$ in the streamwise direction and $0.8D$ in the radial direction. The measurement domain was made of 330 measurement points or nodes. Specifically, this domain was subdivided into 30 measurement planes in the streamwise (X) direction, with each plane consisting of 11 measurement nodes in the radial (R) direction. This procedure resulted in a spacing of 4.064 mm between each measurement node. The uncertainty in the spatial location of these nodes was ± 0.102 mm, whereas the experimental uncertainties in the streamwise and radial velocity components were determined to be 5.0 and 6.1%, respectively. Similarly, the Reynolds stress and vorticity had estimated uncertainties of 6.8 and 13%.

The eduction of the coherent structures was obtained using the life cycle method,[10] which uses a double decomposition representation. This method of conditional sampling and phase averaging utilizes the complete time series from both the measurement probe (the X-wire) and the reference probe.

After careful structure identification and selection, phase averaging is applied by means of structure phase alignment. In this procedure, the time average of the reference signal was used to establish the threshold level for both triggering and cycle determination. Specifically, when the reference wire output signal shows a positive signal value, traveling across the preset threshold level, that location is marked as the beginning of a cycle. The end of the cycle is determined when the reference signal shows a second positive going crossing. This establishes the beginning and end of each cycle in the time series. In a similar manner, the corresponding X-wire time series is also marked and saved as multiple cycles. The life cycle in the present study consisted of 30 phase points ($i = 1$–30). Therefore, each phase point represents part of the total cycle, i.e., the fraction of time that has elapsed.

The preset threshold level utilized was selected after an evaluation of two different sampling criteria: 1) a constant voltage threshold level and 2) a threshold level based on the time-averaged voltage. In the first method, a constant voltage level is selected and used to mark the beginning of each cycle. Four constant voltage levels were chosen for evaluation: 4.50, 4.53, 4.54, and 4.56 V. In all four cases, vortical structures were educed; however, the number of cycles that would make up the ensembles varied. Higher threshold levels resulted in larger educed structures and a smaller number of cycles contributing to the ensemble. Similarly, low-threshold levels produced the opposite effect, i.e., a smaller structure but a larger number of cycles. For the case of 4.56 V, the number of acquired cycles over the total measurement grid varied between 17 and 25.

On average, this only represented 4% of the total reference wire signal. In the 4.50-V case, 199–220 cycles were recorded over the same measurement grid, representing approximately 40% of the flow. Although a greater number of cycles were obtained, the educed structure was determined to be smaller than the typical structure. To try and account for the dynamic changes in a typical vortical structure, at each spatial location, the time average of the reference wire signal was evaluated. This method was also able to produce robust structures and accounted for approximately 28% of the flow, based on the reference wire signal.

In the following sections, comments based on phase-averaged (coherent) flow quantities (i.e., vorticity, velocity, turbulent intensity, Reynolds stress, shear production and strain rate) using the life cycle method are presented. Three distinct regions are identified and examined. They are referred to as 1) the tongue region, 2) region of vortex formation, and 3) the decay region.[10] Note that the magnitude of vorticity displayed in the present contours has been nondimensionalized by the dominant frequency f_m. In a similar manner, the coherent Reynolds stress has been nondimensionalized by $(U_{cl})^2$, the strain rate by f_m, and the coherent shear production by the quantity $f_m(U_{cl})^2$.

Observations

The following recorded observations were based primarily on the visual inspection of the vorticity contour plots. This examination highlighted three distinct vortical regions the character of which is also supported by contours of other coherent flow quantities. Because coherent structure activity is not constant throughout its life cycle, five key coherent vorticity contours will be presented. The temporal order in which the vorticity contours were sampled is represented by phase points, $i = 2$, 7, 12, 17, and 29 (Figs. 3, 4, 5, 6 and 7, respectively). However, for the following discussion, which only seeks to identify key features of these contours, this order will be modified. In addition, contours of normalized coherent Reynolds stress, coherent shear production, and coherent strain rate for phase point, $i = 12$ have been included (Figs. 8–10).

Tongue Region

This initial region begins at the exit of the delivery tube and extends downstream to approximately $X/D = 0.85$ (see phase point $i = 12$, Fig. 5). High levels of concentrated vorticity, characteristic of the tongue region, are readily visible. Such a region of highly concentrated coherent vorticity was also observed by Disimile[3,11]

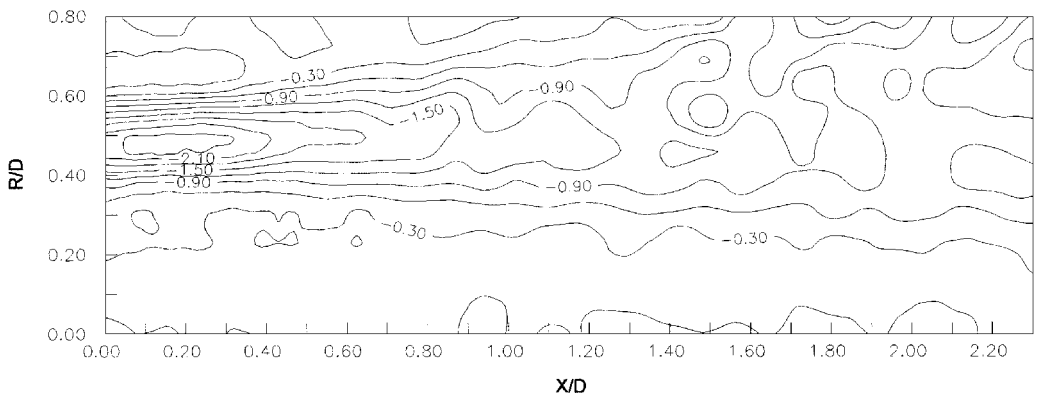

Fig. 3 Nondimensional coherent vorticity $\langle\omega\rangle_i$ at phase point $i = 2$.

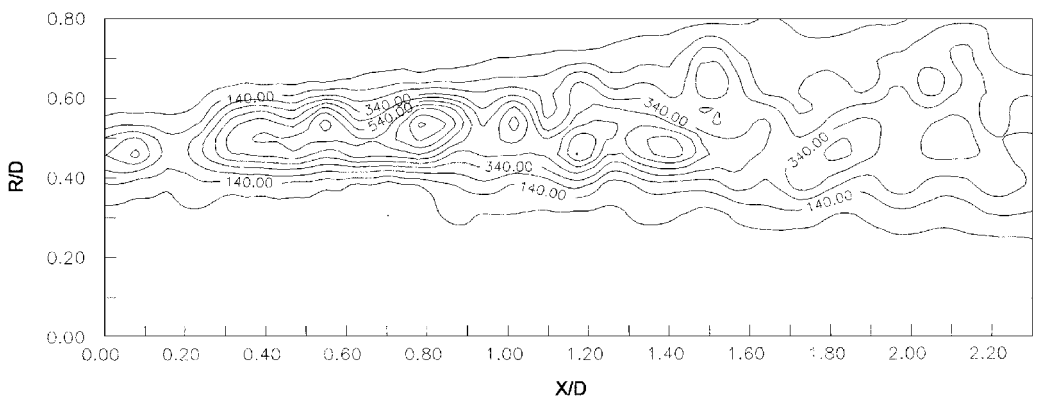

Fig. 4 Nondimensional coherent vorticity $\langle\omega\rangle_i$ at phase point $i = 7$.

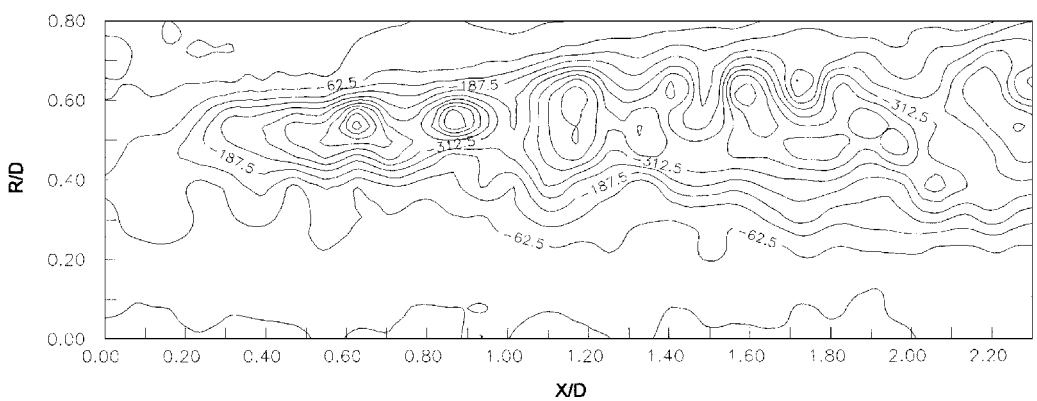

Fig. 5 Nondimensional coherent vorticity $\langle\omega\rangle_i$ at phase point $i = 12$.

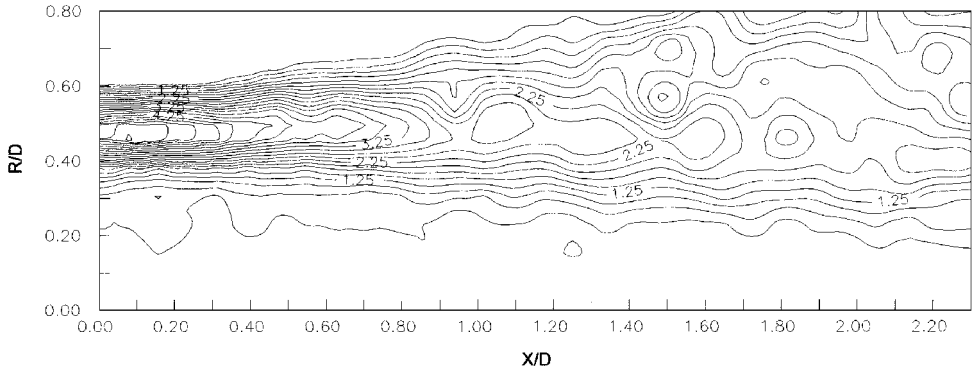

Fig. 6 Nondimensional coherent vorticity $\langle\omega\rangle_i$ at phase point $i = 17$.

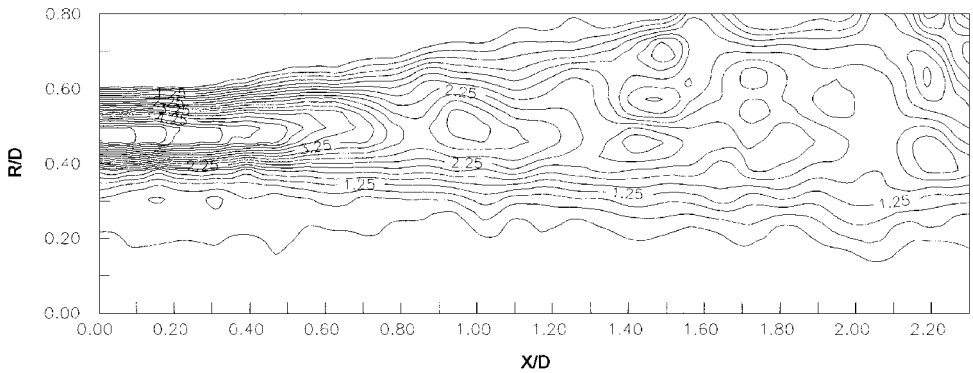

Fig. 7 Nondimensional coherent vorticity $\langle\omega\rangle_i$ at phase point $i = 29$.

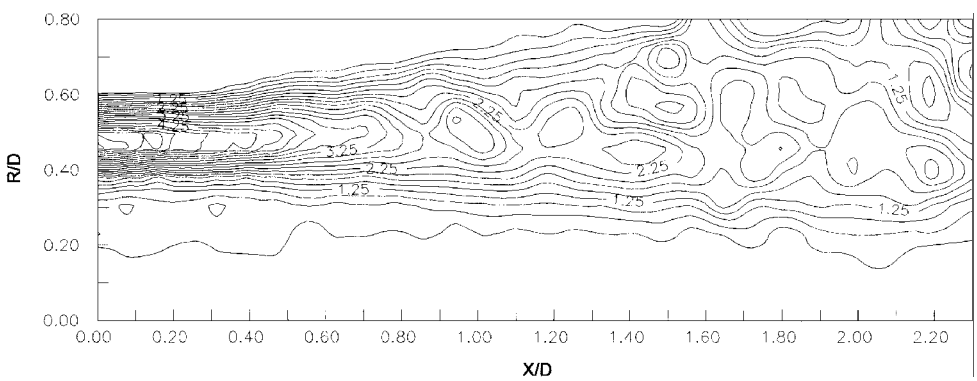

Fig. 8 Nondimensional coherent Reynolds stress $\langle u'v'\rangle_i$ at phase point $i = 12$.

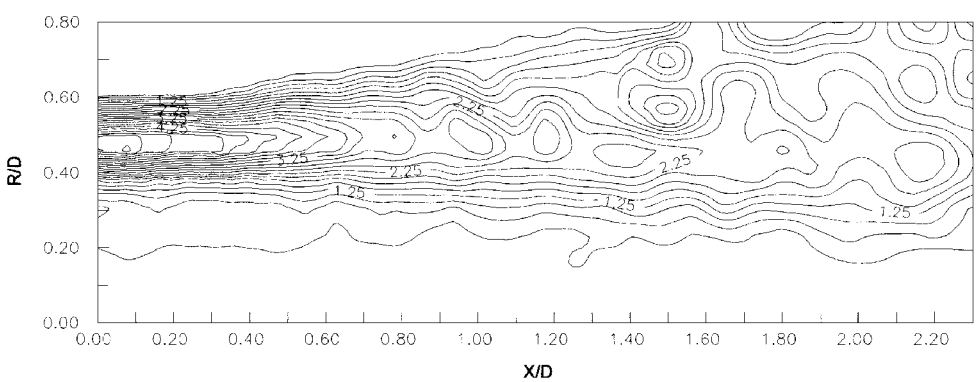

Fig. 9 Nondimensional coherent shear production $\langle P\rangle_i$ at phase point $i = 12$.

in a weakly excited planar free shear layer and is called the tongue region. Within this region, no definable large coherent structures are observed. This agrees with earlier shear layer studies that also reported an absence of large coherent structures immediately downstream of the nozzle exit. These tightly packed contours of high vorticity are an indication of the potential for the downstream formation of large-scale structures. Also observed within this region, up to $X/D = 0.6$, are corresponding high levels of coherent Reynolds stress (Fig. 8). In addition, a careful examination of the coherent streamwise velocity contours[12] $\langle U\rangle_i$ shows a sudden jump in the shear layer thickness and a prelude to vortex formation at approximately $X/D = 0.35$.

Vortex Formation Region

Farther downstream, as can be observed in Fig. 4 ($i = 7$), the region of vortex formation is noted. This region is found between

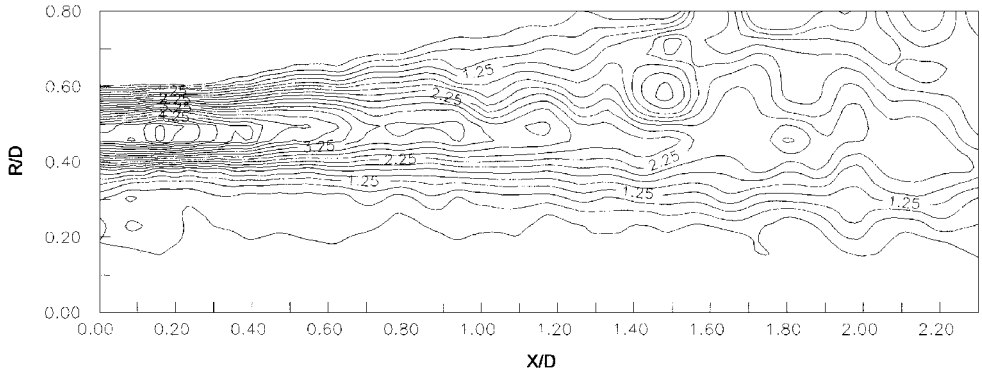

Fig. 10 Nondimensional coherent strain rate $\langle S\rangle_i$ at phase point $i = 12$.

$X/D = 0.85$ and 1.60. Within this region, large isolated coherent structures are observed to form, grow, and convect downstream. A variety of locations have been reported in the literature for the beginning of this region. This variation is believed to be due to the different jet initial conditions and Reynolds numbers.[13,14] For free axisymmetric jets, Yule[8] reports $X/D = 4.5$, whereas Hussain and Zedan[15] note $X/D = 3.3$. Zaman and Hussain[13] report that the shear layer activity, i.e., vortical structure signatures, can be felt on the jet centerline as early as $X/D = 1.5$. For the current experimental configuration, the region of vortex formation starts very early. This observation was expected, first, due to the existence of a highly perturbed jet central region at the delivery tube exit. Such a flow condition is not representative of a jet potential core stemming from a converging nozzle. Therefore, the necessary instabilities for vortex formation exist closer to the delivery tube exit in the present study. Second, in the current case the jet impinges on a plate placed four diameters downstream from the tube exit, $L/D = 4$. Although the flow speed in the present study is low, there may still be a small feedback influence due to the presence of the plate. Several researchers have noted that a feedback effect from the downstream plate alters the flowfield upstream to some degree.[4,16,17] Ho and Nosseir[16] report that this feedback deforms the shear layer and alters the coherent structure formation, especially at high Reynolds numbers. Third, it is well documented that a turbulent shear flow persists shorter distances downstream than a laminar shear flow.[6] This implies that the higher the level of upstream turbulence, the shorter the downstream persistence of the coherent structures. Therefore, it is expected that this highly turbulent jet emanating from the delivery tube should result in reduced distances of coherent structure existence compared with that found in jets with an undisturbed central core.

Decay Region

Unlike the region of vortex formation, the characteristics in the decay region are poorly phase correlated and scattered (Fig. 5, $i = 12$). This region of declining coherent vorticity can be estimated to begin at $X/D = 1.6$ and extend downstream beyond $X/D = 2.3$. Decay is attributed to the dilution and eventual destruction of coherent vorticity by background turbulence.[18] As seen from the coherent vorticity contours, the decay region is easily identified by the large regions of nonconcentric contours of relatively low-level vorticity. The large-scale coherent structures, developed in the upstream region, are being diluted and destroyed by the high levels of Reynolds stress and result in increased turbulent production. That is, the transfer of energy apparently from coherent to incoherent motions can be attributed to the deformation work done by the Reynolds stress.[19]

Coherent Vortex Dynamics

The results of the life cycle method will be utilized to study the coherent vortex dynamics in the near field of this jet flow. First, the coherent vorticity equation will be investigated. Second, a general discussion based on the phase-averaged contour plots for vorticity, velocity, turbulent intensity, Reynolds stress, shear production, and strain rate will be presented.

Phase-Averaged Coherent Vorticity Equation

The coherent vorticity equation will be examined term by term at several phase points and physical locations. This will provide a better understanding of each term and its physical significance on the coherent vorticity dynamics in the present configuration.

Using the assumptions $\partial/\partial\theta \approx 0$ and $u_\Theta \approx 0$, the reduced coherent vorticity equation in cylindrical coordinates (R, θ, X) is presented. An order of magnitude analysis was also performed on each term of the coherent vorticity equation. Results obtained for the right-hand side (RHS) of the equation are given below each term:

$$\frac{D\langle\omega\rangle}{Dt} = \frac{1}{Re}\left[\frac{\partial^2\langle S\rangle}{\partial x^2} - 2\frac{\partial^3\langle U\rangle}{\partial x^2\partial r} + \frac{\partial^2\langle S\rangle}{\partial r^2} - 2\frac{\partial^3\langle U\rangle}{\partial r^3} + \frac{1}{r}\frac{\partial\langle S\rangle}{\partial r}\right.$$
$$\mathcal{O}(10^{-2}) \quad \mathcal{O}(10^{-7}) \quad \mathcal{O}(10^{-2}) \quad \mathcal{O}(10^{-1}) \quad \mathcal{O}(10^{-2})$$
$$\left. - \frac{2}{r}\frac{\partial^2\langle U\rangle}{\partial r^2}\right] - \frac{\partial^2}{\partial x^2}\langle u'v'\rangle + \frac{\partial^2}{\partial r^2}\langle u'v'\rangle + \frac{1}{r}\frac{\partial}{\partial r}\langle u'v'\rangle$$
$$\mathcal{O}(10^{-2}) \quad \mathcal{O}(1) \quad \mathcal{O}(1) \quad \mathcal{O}(10^{-1})$$

where $\langle\omega\rangle$, $\langle S\rangle$, $\langle U\rangle$, and $\langle u'v'\rangle$ are the phase-averaged vorticity, strain rate, velocity, and Reynolds stress, respectively. The left-hand side (LHS) of the coherent vorticity equation was also evaluated using Taylor's hypothesis

$$\frac{\partial}{\partial t} \approx \langle U_C\rangle\frac{\partial}{\partial x}$$

As a result, the LHS of the coherent vorticity equation then becomes

$$\text{LHS} = [\langle U\rangle + \langle U_C\rangle]\frac{\partial\langle\omega\rangle}{\partial x} + \langle V\rangle\frac{\partial\langle\omega\rangle}{\partial r}$$
$$\mathcal{O}(1) \quad \mathcal{O}(1)$$

Retaining terms with high order of magnitude, i.e., $\geq \mathcal{O}(0.1)$, a reduced coherent vorticity equation can be rewritten as

$$[\langle U\rangle + \langle U_C\rangle]\frac{\partial\langle\Omega\rangle}{\partial x} + \langle V\rangle\frac{\partial\langle\Omega\rangle}{\partial r} = \frac{1}{Re}\left[-2\frac{\partial^3\langle U\rangle}{\partial r^3}\right]$$
$$- \frac{\partial^2}{\partial x^2}\langle u'v'\rangle + \frac{\partial^2}{\partial r^2}\langle u'v'\rangle + \frac{1}{r}\frac{\partial}{\partial r}\langle u'v'\rangle$$

These terms were then evaluated by curve fitting the experimental data acquired at many physical locations (X/D, R/D) and at several phase points ($i = 4$, 7, 12, 17, 24, and 30), and the following major findings are reported.

1) Even at this moderate jet Reynolds number ($Re_D = 1.3 \times 10^4$), the effects of viscosity were found to be negligible. The viscous terms were determined to be at least one order of magnitude smaller than the nonviscous terms. Estimations performed at several locations generally found that the ratio of nonviscous to viscous terms varied randomly. Throughout the flowfield, typical values ranging between 11 and 50 were estimated.

2) The second derivatives of the Reynolds stress were found to be the most dominant terms on the RHS of the coherent vorticity equation. The direct effect of the Reynolds stress distribution on

the coherent vorticity at this moderate Reynolds number was highlighted. The same conclusion was also reached by Hussain[4] from pure dimensional analysis and a high Reynolds number assumption.

3) In general, the difference between LHS and RHS of the coherent vorticity equation is slightly higher within the core of the coherent structure and decreases as one moves away from the center of the core. A comparison of the LHS and RHS of the reduced coherent vorticity equation shows agreement ranging between 2% (best case) and 67% (worst case). Evaluating the experimentally acquired data from randomly chosen spatial locations and phase points, an average difference of 33% between both sides of the reduced coherent vorticity equation was estimated.

It is felt that this difference may be in part due to the inapplicability of Taylor's hypothesis, which was used in the calculation of the LHS of the vorticity equation because there are high levels of $\langle u' \rangle$ in the core region. Hussain[4] reported that the longitudinal turbulent intensity must be small for the successful application of the Taylor hypothesis. To obtain a simple measure of the difference resulting from the application of Taylor's hypothesis, the reduced coherent vorticity equation is rearranged and the term representing Taylor's hypothesis is solved for

$$\langle U_C \rangle \frac{\partial \langle \Omega \rangle}{\partial x}$$

The uncertainty is then given by the absolute value of the difference between the preceding term and all remaining terms in the reduced vorticity equation. Excluding eight data points, this resulted in differences ranging from 0.5 and 69.4%. Accounting for the eight excluded data points, errors as high as 386% were noted.

Coherent Vorticity Redistribution

One of the salient features of the vorticity contours is the drop in the peak phase-averaged vorticity levels in the middle of the shear layer with increasing downstream distance. For instance, at phase point $i = 12$ (Fig. 5), the nondimensional peak vorticity level in the center of the shear layer is approximately 5.85 at $X/D = 0.03$, 4.15 at $X/D = 0.48$, 3.17 at $X/D = 0.9$, and finally 2.68 at $X/D = 1.4$. Similar decreases in vorticity were also observed by other researchers for axisymmetric as well as plane free shear layers.[7,8,11,18,20] Likewise, peaks in both the coherent production by background turbulence and coherent momentum transport by background turbulence terms in the energy equation were also seen to decrease in magnitude with increasing X/D. Therefore, lower levels of coherent vorticity, coherent production, and coherent momentum transport are consistently observed as one moves downstream. One reason for this streamwise decrease in the vorticity level is the redistribution of vorticity via jet spreading. This is self-evident from the coherent vorticity contour plots. The redistribution of coherent vorticity by means of the Reynolds stress is inferred because it was shown to be the only dominant term remaining in the coherent vorticity equation. This finding, coherent vorticity dilution due to high levels of Reynolds stress, was also noted by previous researchers.[4,8] Additional support for this is found in the phase-averaged energy equation. Specifically, the coherent momentum transport term has broader and broader profiles as the fluid moves downstream.[12] Additionally, a phase lag is observed, that is, the zones of high Reynolds stress indicate a dilution effect after some time. This means if high magnitudes of $\langle u'v' \rangle$ were observed in the structure core at one particular phase point, only at a later phase point would one notice coherent structure dilution. For instance, at phase point $i = 12$ (Fig. 5), there is approximately a 0.24 drop in the nondimensional phase-averaged vorticity level in the second structure. This loss is related to the high magnitudes of Reynolds stress that were observed in the center of the second structure during earlier phase points. This observation suggests that flow required time to adjust and the effect only becomes apparent at later phase points. Therefore, to thoroughly understand the dynamics of jet turbulence, an examination of the time evolution of several flow characteristics, i.e., the utilization of a double decomposition, is essential.[15] Otherwise, valuable information can be lost or misinterpreted using a time-averaged treatment of the governing equations.

Vortex Formation, Growth, and Interaction

Vorticity dynamics (vortex formation, growth, their downstream convection and interaction, etc.) is investigated phase point by phase point using phase-averaged flow quantities. Analysis of vortex dynamics in the decay region is difficult due to the three dimensionality and scatter of the data that exist within this region. Therefore, the following discussion will focus on the first two regions: the tongue and vortex formation regions.

Coherent structure formation is presented in Fig. 3, phase point $i = 2$. Sudden changes in the slope of the several phase-averaged vorticity contour lines, i.e., their waviness, are observed at approximately $(X/D, R/D) = (0.92, 0.50)$ and $(1.2, 0.50)$. Changes at $X/D = 0.92$ are manifestations of the structures that are about to be born. In addition, the observed fluctuations, particularly in $\langle u'v' \rangle$ and $\langle V \rangle$, within the tongue region are also signatures of the instabilities needed for vortex formation.[4,6] At this phase point, the distinction between the tongue and region of vortex formation is unclear. Contours of phase-averaged vorticity are observed to be very straight and similar to time-averaged vorticity contours up to about $R/D = 0.52$. However, the decay region, even at this early phase point, has a very different character, i.e., the vorticity is relatively constant, dispersed, and poorly phase correlated. A similar decay character due to the large scatter in data representing the coherent production by background turbulence and the coherent momentum transport by background turbulence terms[12] is also noticeable.

Five phase points later, i.e., after 2.5 ms, at phase point $i = 7$ (Fig. 4), the coherent structures are observed to grow in size and strength. The peak vorticity level in the core of each structure is approximately 3.17, 2.93, and 2.44 for the first, second, and third structures, respectively. This growth in the vortical structures is believed to be due to the low Reynolds stress level, i.e., the local valley in the $\langle u'v' \rangle$ contours, experienced in the structures core. At this phase point, the redistribution of vorticity within the coherent structures by the high levels of Reynolds stress (in the second and third structures) is not yet apparent. As already mentioned, the peak $\langle u'v' \rangle$ levels are expected to reduce the strength of the coherent structures.[4,8] Further, this effect is not immediate and will be observed at a later phase point. A look at the coherent energy equation, for the same phase point, indicates that there was an increase in the phase-averaged energy convected from $X/D = 0.5$ to 1.0, while the coherent production by the background turbulence was maintained at approximately the same levels. Inside and outside the structures, the effects of viscosity are still negligible. At this particular phase point ($i = 7$), the coherent momentum transport by background turbulence is found to be lower in the tongue region than in the region of vortex formation. Momentum transport also drops as one moves downstream from $X/D = 0.5$ to 1.0. However, at $X/D = 1.5$, the coherent momentum transport returns to levels higher than those at $X/D = 0.5$. Therefore, during the process of vortex formation, an increase in the coherent momentum transport is observed.

At phase point $i = 12$, the initial structure, i.e., the first large-scale motion closest to the tube exit, continues to grow in size, reaching about $0.25D$. By comparing Figs. 5, 8, and 9, coherent structure growth can be observed between the peak Reynolds stress and coherent shear production regions, i.e., around the valleys of $\langle u'v' \rangle$ and $\langle P \rangle$. A similar finding was also reported for excited shear layers.[11,21] This observation agrees with the earlier finding from the phase-averaged vorticity equation, i.e., the second derivative of the Reynolds stress plays the dominant role in coherent vorticity dynamics. A valley in the coherent strain rate distribution was also observed at the same location (Fig. 10). None of the other phase-averaged quantities (coherent velocity, turbulent intensity, etc.) shows any salient features suggesting vortex growth of the first structure. Therefore, strong vortex growth is observed 1) in the valley of coherent shear production (within this region less energy is consumed by the incoherent turbulence); 2) downstream or between regions of peak coherent Reynolds stress, i.e., in the $\langle u'v' \rangle$ valley; and 3) in the valley of the coherent strain rate.

An examination of the phase-averaged vorticity contour at $i = 12$ (Fig. 5) yields information suggesting that the first structure is tilted about 45 deg, i.e., the orientation of its major axis, with respect to the flow direction. Such a tilting of coherent structures was also

observed by Tso and Hussain.[5] This tilting is believed to be related to the strain rate and, as pointed out by Hussain and Zaman,[18] its final adjustment should be with the main flow gradient. Indeed, this final adjustment, i.e., coherent structure main axis being aligned with the main flow direction, is apparent in Fig. 7, phase point $i = 29$. At this phase point, the second and third structures are seen to be diluted due to the production of the incoherent turbulence by the high $\langle u'v' \rangle$ levels that were observed within these structures at earlier phase points. The support for this comes from the comparison of the phase-averaged shear production plot (Fig. 9) and the phase-averaged vorticity plot (Fig. 5). Because the double decomposition can be thought of as the incoherent (or random) component riding on top of coherent, i.e., periodic, flow, production relates to the mechanism of energy transfer from coherent to incoherent motions. Recall, low turbulence production was also noted in the center of the first coherent structure, i.e., less incoherent turbulence being created, as it grows in size, while simultaneously high production of the incoherent turbulence in the center of the second and third structures was observed.

At phase point $i = 17$ (Fig. 6), the only surviving large coherent structure in the near field is elongated and tilted and is beginning to align itself with the streamwise direction. Yet structure growth continues due to the low levels of shear production within that region. According to Fiedler,[14] the vortex cross section is deformed and, eventually, its main axis is aligned with the axis of the principal strain and this is its most deterministic direction. Further, as the Reynolds number increases, the structures become stronger and more rounded. Therefore, the elongated structure shape, as observed in the present study, is expected due to the moderate Reynolds number. The large-scale coherent structure reaches its largest size of about $0.4D$ (in streamwise extent). Even though the initial conditions are different, the current coherent structure size is comparable with Zaman and Hussain's[13] and Yule's[8] results for axisymmetric freejets. They found the structure size to be about $0.5D$ at $X/D = 3$ and about $0.4D$ at $X/D = 4.5$, respectively. Their coherent structures were also located in the middle of the shear layer, as in the current case. This means Lau's two street coherent structure model[13] (which argues that there are two coherent structures in the jet shear layer moving side by side) does not find any support from the current study either. The only remaining coherent structure generates a second peak at the same location where a valley in the $\langle u'v' \rangle$ and $\langle P \rangle$ contours were observed. This finding is interesting because the coherent structure first becomes large and elongated and then, due to the low Reynolds stress and strain rate levels, develops a second peak. Because the structure is too elongated, it is unable to keep its oneness and splits. Eventually, as the structure moves downstream decay will occur.

Approaching the last phase point, $i = 29$ (Fig. 7), the end of the life cycle is near, the coherent structure's strength and size decrease, which represents the decay and break up of the large organized vortical structures. As expected, the cycle repeats, a new coherent structure is born, and the vorticity field is once again represented by the initial phase points, e.g., $i = 2$ (Fig. 3).

Convection Velocity

The average convection velocity of the coherent structure can be estimated using the phase-averaged vorticity contours. Tracking the position of the first structure from $X/D = 1.04$ at phase point $i = 4$ to $X/D = 1.28$ at phase point $i = 20$ corresponds to a 1.22-cm movement in a time interval of 8 ms. This equates to an estimated average coherent structure convection velocity (U_C) of 1.52 m/s, which compares to the measured value to within 10%. The measured convection velocity of the large-scale structure, 1.68 m/s, was determined from the time average of the streamwise velocity component at the structure center. This small difference is attributable to 1) the different size structures present in the flowfield, 2) the acceleration and deceleration of the structures while traveling downstream as already noted,[7,8,11] and 3) alignment of the different size structures during the eduction of the typical structure.

The spacing (or the wavelength) between the large coherent structures was also estimated from the vorticity contours and determined to be approximately $0.43D$. At a central location within the coherent structure an average streamwise velocity of approximately 42% of the centerline velocity ($U_{cl} = 4.0$ m/s) was determined. Performing FFTs on the hot-wire signals, it was determined that the dominant vortex shedding frequency f_m was 82 Hz. This is very close to the 66 Hz that was related to the time scale for the life of a typical large-scale structure, i.e., the life cycle period. As a verification of the structure wavelength, the dominant time scale ($1/f_m$) and measured convection velocity were used to calculate the coherent structure wavelength. This resulted in a wavelength of $0.418D$. If, instead, the time scale based on the life cycle method was used, a spacing approximately 20% larger would be obtained.

Coherent Structure Growth

It is possible to get some insight on the growth rate of the coherent structure by a direct area measurement using the topological phase-averaged vorticity contours. For this purpose, the area surrounded by the vorticity contour level 2.50 of the first structure was measured using graphical integration at each phase point. The size of the first coherent structure increases almost linearly by as much as 34% until phase point $i = 17$, beyond which point the typical structure begins to shrink.

Winant and Browand[22] report that they observed pairing at moderate Reynolds numbers. However, there was no pairing observed in the current jet near field. This agrees with Zaman and Hussain's[13] claim that pairing is observed for the laminar jet but not for the turbulent jet case. Therefore, no smearing due to pairing is present in the educed structures.[5,7] Similarly, no vortex merging was observed in the current study. According to Fiedler,[14] vortex mergers are not expected in a natural free shear layer.

Summary

After careful examination of the educed coherent structures and the terms in the coherent vorticity equation in the jet near field, the following observations are reported.

1) Phase-averaged vorticity contours suggest the existence of large coherent structures in the jet near field. The first large coherent structure is formed at about one diameter downstream of the delivery tube exit with an approximate core size of $0.4D$.

2) Even at the moderate Reynolds number of 1.3×10^4, the influence of viscosity on the vorticity dynamics of the large vortical structures is shown to be negligible.

3) Through shear production, the peak Reynolds stress is observed to slowly dilute and destroy the large-scale organized structures within the shear layer.

4) Near-field coherent structures in the current, fully turbulent jet were observed to grow at locations where a valley in coherent shear production was observed. This also corresponded to regions in the flowfield where Reynolds stress and strain rate levels were minimal.

5) The use of Taylor's hypothesis is found to produce poor results in the region around the core of the coherent structure.

References

[1]Hussain, A. K. M. F., "Large Scale Organized Motions in Jets and Shear Layers," *Recent Advances in Aerodynamics*, edited by A. Krothapalli and C. A. Smith, Springer–Verlag, New York, 1986, pp. 205–262.

[2]Oler, J. W., and Goldschmidt, V. W., "Coherent Structures in the Similarity Region of Two Dimensional Turbulent Jets," *Journal of Fluids Engineering*, Vol. 106, No. 2, 1984, pp. 187–192.

[3]Disimile, P. J., "Phase Averaged Transverse Vorticity Measurements in an Excited, Two Dimensional Mixing Layer," *AIAA Journal*, Vol. 24, No. 10, 1986, pp. 1621–1627.

[4]Hussain, A. K. M. F., "Coherent Structures, Reality and Myth," *Physics of Fluids*, Vol. 26, No. 10, 1983, pp. 2816–2850.

[5]Tso, J., and Hussain, F., "Organized Motions in a Fully Developed Turbulent Axisymmetric Jet," *Journal of Fluid Mechanics*, Vol. 203, 1989, pp. 425–448.

[6]Liu, J. T. C., "Large Scale Coherent Structures in Free Turbulent Flows and Their Aerodynamic Sound," *Recent Advances in Aerodynamics*, edited by A. Krothapali and C. A. Smith, Springer–Verlag, New York, 1986, pp. 297–334.

[7]Bruun, H. H., "A Time Domain Analysis of the Large Scale Flow Structure in a Circular Jet, Part 1. Moderate Reynolds Number," *Journal of Fluid Mechanics*, Vol. 83, No. 4, 1977, pp. 641–671.

[8]Yule, A. J., "Large Scale Structure in the Mixing Layer of a Round Jet," *Journal of Fluid Mechanics*, Vol. 89, No. 3, 1978, pp. 413–432.

[9]Foss, J. F., Klewicki, C. L., and Disimile, P. J., "Transverse Vorticity Measurements Using an Array of Four Hot-Wire Probes," NASA CR-178098, May 1986.

[10]Aydore, S., and Disimile, P. J., "A New Method for the Eduction of the Natural Coherent Structures," *AIAA Journal*, Vol. 33, No. 8, 1995, pp. 1529–1531.

[11]Disimile, P. J., "Transverse Vorticity Measurements in an Excited Two Dimensional Mixing Layer," Ph.D. Thesis, Dept. of Mechanical Engineering, Michigan State Univ., East Lansing, MI, June 1984.

[12]Aydore, S., "Investigation of Large Coherent Structures in the Near Field of an Impinging Axisymmetric Jet," Ph.D. Thesis, Dept. of Aerospace Engineering, Univ. of Cincinnati, Cincinnati, OH, July 1991.

[13]Zaman, K. B. M. Q., and Hussain, A. K. M. F., "Natural Large Scale Structures in the Axisymmetric Mixing Layer," *Journal of Fluid Mechanics*, Vol. 138, 1984, pp. 325–351.

[14]Fiedler, H. E., "Initiation, Evolution and Global Consequences of Coherent Structures in Turbulent Shear Flows," *Proceedings of the Symposium on Coherent Structures* (Madrid, Spain), Vol. 136, Springer–Verlag, 1980.

[15]Hussain, A. K. M. F., and Zedan, M. F., "Effects of the Initial Condition on the Axisymmetric Free Shear Layer: Effect of the Initial Momentum Thickness," *Physics of Fluids*, Vol. 21, 1978, pp. 1100–1112.

[16]Ho, C. M., and Nosseir, N. S., "Dynamics of an Impinging Jet. Part 1. The Feedback Phenomenon," *Journal of Fluid Mechanics*, Vol. 105, 1981, pp. 119–142.

[17]Jimenez, J. (ed.), *The Role of Coherent Structures in Modeling Turbulence and Mixing*, Vol. 136, Springer–Verlag, Berlin, 1980, pp. 10–304.

[18]Hussain, A. K. M. F., and Zaman, K. B. M. Q., "Vortex Pairing in a Circular Jet Under Controlled Excitation. Part 2. Coherent Structure Dynamics," *Journal of Fluid Mechanics*, Vol. 101, No. 3, 1980, pp. 493–544.

[19]Tennekes, H., and Lumley, J. L., *A First Course in Turbulence*, MIT Press, Cambridge, MA, 1972, Chap. 2.

[20]Curlett, B. P., and Disimile, P. J., "Phase Averaged Transverse Vorticity Measurements in an Excited Two Dimensional Slit Jet," AIAA Paper 88-0041, Jan. 1986.

[21]Curlett, B. P., "An Experimental Investigation of an Unconfined, Acoustically Excited Slit-Jet Flow Field," M.S. Thesis, Aerospace Engineering and Engineering Mechanics Dept., Univ. of Cincinnati, Cincinnati, OH, June 1987.

[22]Winant, C. D., and Browand, F. K., "Pairing of Coherent Structures," *Journal of Fluid Mechanics*, Vol. 63, 1974, pp. 23–27.

F. W. Chambers
Associate Editor